

Theory of Acceleration of Decision Making by Correlated Time Sequences

Norihiro Okada,¹ Tomoki Yamagami,² Nicolas Chauvet,² Yusuke Ito,¹ Mikio Hasegawa,¹ and Makoto Naruse²

¹ *Department of Electrical Engineering, Graduate School of Engineering, Tokyo University of Science, 6-3-1 Nijuku, Katsushika-ku, Tokyo 125-8585, Japan*

² *Department of Information Physics and Computing, Graduate School of Information Science and Technology, The University of Tokyo, 7-3-1 Hongo, Bunkyo-ku, Tokyo 113-8656, Japan*

Abstract

Photonic accelerators have been intensively studied to provide enhanced information processing capability to benefit from the unique attributes of physical processes. Recently, it has been reported that chaotically oscillating ultrafast time series from a laser, called laser chaos, provides the ability to solve multi-armed bandit (MAB) problems or decision-making problems at GHz order. Furthermore, it has been confirmed that the negatively correlated time-domain structure of laser chaos contributes to the acceleration of decision-making. However, the underlying mechanism of why decision-making is accelerated by correlated time series is unknown. In this paper, we demonstrate a theoretical model to account for the acceleration of decision-making by correlated time sequence. We first confirm the effectiveness of the negative autocorrelation inherent in time series for solving two-armed bandit problems using Fourier transform surrogate methods. We propose a theoretical model that concerns the correlated time series subjected to the decision-making system and the internal status of the system therein in a unified manner, inspired by correlated random walks. We demonstrate that the performance derived analytically by the theory agrees well with the numerical simulations, which confirms the validity of the proposed model and leads to optimal system design. The present study paves the new way for the effectiveness of correlated time series for decision-making, impacting artificial intelligence and other applications.

1. Introduction

Optics and photonics have been extensively studied for high-speed information processing in various applications, especially machine learning [1–5]. One of the important branches of research frontier is reinforcement learning [6], wherein the impacts of photonics have been intensively examined [7–9]. The multi-armed bandit (MAB) problem regards decision-making in obtaining high rewards from multiple selections, called *arms*, wherein the best arm is initially unknown. MAB problems concern a difficult tradeoff known as exploration-exploitation dilemma, which captures a fundamental aspect of reinforcement learning [6].

The physical properties of photons have been utilized in solving MAB problems [7,8]. Especially, chaotically oscillating ultrafast time series generated by semiconductor lasers, called laser chaos, have been successfully utilized in resolving two-armed bandit problems in GHz order, which we call laser chaos decision-maker hereafter [7]. As introduced below, the principle of laser chaos decision-maker simply depends on the signal level comparison between the chaotically oscillating time series and the threshold level. It has also been demonstrated

that such a level-comparison-based principle is scalable in a tree architecture, experimentally demonstrated up to 64 arms [10].

Furthermore, the applications of laser chaos decision-makers have been studied to benefit from its prompt adaptation abilities in dynamically changing uncertain environments [11–14]. Takeuchi *et al.* applied laser chaos decision-making to channel selection problems in wireless communications [11], in which communication channels suffer from dynamically changing disturbances due to traffic, interference, or fading [15]. Kanemasa *et al.* extended the principle using laser chaos decision-maker to channel bonding in IEEE802.11ac networks [12]. Further, Duan *et al.* optimized user pairing in non-orthogonal multiple access (NOMA) systems by laser chaos decision-maker [13]. Moreover, Kanno *et al.* combined laser chaos-based decision-making with photonic reservoir computing, where adaptive model selection is realized to enhance the computing capability [14].

In [7], it has been demonstrated that the autocorrelation inherent in laser chaos time series impacted the decision-making performances. Indeed, chaotic time series with negative maximum autocorrelation yield superior performances compared with pseudorandom numbers, colored noise, and random shuffle surrogate data of the original laser chaos time series [7]. Furthermore, Okada *et al.* extensively examined the decision-making acceleration by laser chaos by surrogate analysis such as Fourier transform surrogate [16]. It was found that both statistical distributions of the amplitude of time series and negative autocorrelation therein impact decision-making performances [16].

In the literature, the usefulness of negative autocorrelation in time series has been theoretically analyzed regarding code division multiple access (CDMA) [17–19]. In order to achieve high performance in CDMA, the cross-correlation between the spreading sequences must be small. The optimal negative autocorrelation to minimize the interference has been mathematically derived; the chaotic map that generates the smallest cross-correlation was defined [19]. An FIR filter to generate the optimal chaotic CDMA sequence was also proposed based on the negative autocorrelation analysis [20]. Moreover, the effectiveness of such optimal negative autocorrelation codes has been experimentally demonstrated using software-defined radio systems [21].

However, about decision-making, the fundamental underlying mechanism of how negative autocorrelation inherent in time series impacts the performance superiority is still not understood. That is, the results in the former studies [7,16] are all limited in empirical findings. If the effectiveness of the negative autocorrelation in laser chaos or correlated time series for decision-making is theoretically grasped, it allows, for example, a systematic design approach to derive the optimal autocorrelation depending on given problem situations. Besides, the insights gained by mathematical modeling ensure the reliability of the effectiveness provided by the negative autocorrelation in time series.

In this paper, we theoretically construct a model to account for the effect of negative autocorrelation in decision-making performances. The theory of the present study is inspired by correlated random walk [22,23]. While the transition probabilities of conventional random walks do not depend on previous events, those of correlated random walks do depend on the previous event [22,23]. That is, the notion of correlated random walks allows to represent state-dependent, different probability evolution dynamics. Such a theoretical architecture accounts for the interplay between the correlated time series and the evolution of decision-making. We clarify the validity of the proposed theoretical model by confirming the excellent agreement of

the decision-making performances derived analytically by the proposed model and by numerical simulations.

The rest of the paper consists of the following. [Section 2](#) reviews the mechanism of laser chaos decision-maker. In [Section 3](#), we introduce a numerical method to generate an arbitrary autocorrelation in time series, by which the relevance between autocorrelation and the resultant decision-making performance is systematically examined. [Section 4](#), which is the most important contribution of this study, demonstrates the theoretical model of decision-making based on correlated time sequences. [Section 5](#) demonstrates the agreement of the decision-making performances predicted by the proposed theory and numerical simulations. [Section 6](#) concludes the paper.

2. Laser Chaos Decision Maker: Using Time Series for Decision Making

As introduced in [Section 1](#), the laser chaos time series allows ultrafast decision-making. [Figure 1\(a\)](#) schematically illustrates the architecture of the laser chaos decision-maker for a two-arm bandit problem, which is the scope of the present study [\[7\]](#). The two arms are called slot machines A and B. The laser chaos is generated by subjecting a portion of the output light back to the laser by an externally arranged reflector, which is called delayed feedback. We compare the intensity level of the laser chaos with a certain threshold value, which is denoted by $T(t)$.

The decision-making is executed as follows. When the sampled value of the time series is above the threshold, the decision is to choose slot machine A; otherwise, slot machine B is selected. The threshold $T(t)$ is updated according to the result of the slot machine play. Overall, the threshold update is conducted in the concept that the revised threshold will lead to the same decision in the subsequent decisions when the present action is successful, whereas the threshold is revised to the opposite direction when the present action is failed [\[7,8,10\]](#).

More precisely, the values of threshold $T(t)$ are determined by

$$T(t) = k \times [TA(t)], \quad (1)$$

where $TA(t)$ is called the threshold adjuster and $[*]$ denotes round the number $*$ toward zero. $[TA(t)]$ can take an integer value ranging from $-N$ to N with N being a natural number. Therefore, the number of levels that the threshold adjuster can take is $2N + 1$. Here, k is a coefficient to convert $[TA(t)]$ to $T(t)$; in other words, k specifies the width of a unit change of threshold adjuster. Hence, the range of $T(t)$ is between $-kN$ and kN .

$TA(t)$ is updated depending on the result of the action conducted at $t - 1$:

$$\left. \begin{aligned} TA(t) &= -\Delta + \alpha TA(t-1), & \text{if slot machine A wins} \\ TA(t) &= +\Delta + \alpha TA(t-1), & \text{if slot machine B wins} \\ TA(t) &= +\Omega + \alpha TA(t-1), & \text{if slot machine A fails} \\ TA(t) &= -\Omega + \alpha TA(t-1), & \text{if slot machine B fails} \end{aligned} \right\}, \quad (2)$$

where Δ denotes the increment, which is given by $\Delta = 1$ in the present study. α is the forgetting parameter for weighting previous threshold adjuster variables, ranging from 0 to 1; i.e., $0 \leq \alpha \leq 1$. Ω is called the penalty parameter [\[7,8\]](#).

A hierarchical formation of such two-armed bandit problems has been proposed to deal with problems with more than two arms [\[10\]](#). The elemental structure is the abovementioned two-armed situations with a dynamically updated threshold. This study focuses on two-arm situations.

3. Effectiveness of Correlated Time Series on Decision Making

As described in [Section 1](#), the performance of the two-armed bandit problem using laser chaos time series depends on the autocorrelation inherent therein [\[7,16\]](#). The best performance was obtained when the autocorrelation of the time series exhibited its negative maximum [\[7\]](#). Furthermore, the surrogate data analysis of laser chaos time series clarified the impact of time-domain correlation [\[10\]](#). In this study, in order to examine the influence of correlations in time series in a systematic manner, we introduce an artistically constructed time-correlated time series and analyze its influence on decision-making performance.

We construct time series whose amplitude follows a Gaussian distribution while having a determined autocorrelation by utilizing the Fourier transform surrogate method [\[24\]](#):

- (1) Construct a time series $r(t)$ where t ranges from 0 to $T - 1$, meaning that T is the length of the time series. Here we suppose that $r(t) = r(0) \lambda^t$. Namely, $r(t) = \lambda r(t - 1)$ holds, meaning that $r(t)$ undergoes a time correlation specified by λ to its previous point $r(t - 1)$. We call λ the *autocorrelation coefficient* in this study.
- (2) The Fourier transformed of $r(t)$ is calculated, denoted by $R(f)$.
- (3) The phase of $R(f)$ is revised by randomly assigned numbers while the power spectrum is maintained. The revised Fourier-domain signal is denoted by $R'(f)$.
- (4) By conducting inverse Fourier transform of $R'(f)$, a new time series is generated, which is denoted by $r'(t)$.

Through the process above, the autocorrelation of the resultant $r'(t)$ is equivalent to the original autocorrelation $r(t)$. However, the amplitude distribution of $r'(t)$ follows a Gaussian profile thanks to the randomized phase factors in the Fourier domain. The above-described process corresponds to a special case of Fourier transform surrogate [\[24\]](#).

Snapshots of the time series generated are shown regarding the cases when the time correlation is specified by $\lambda = 0.8$, 0, and -0.8 in [Figures 1\(b\), 1\(c\), and 1\(d\)](#), respectively. All of the time series look random, but they contain evidently clear differences in their autocorrelation. With $\lambda = 0.8$, the signal level at time t is similar to the signals around that point; that is, radically large signal-level differences in consecutive data points are rarely observed ([Figure 1\(b\)](#)). Conversely, with $\lambda = -0.8$, meaning a strong negative autocorrelation, the signal at time t is an almost opposite value compared with the data around ([Figure 1\(d\)](#)). As a result, the time series exhibits a highly time-varying structure. In the meantime, the histogram of the signal level of these time series follows the same Gaussian distribution.

It should be noted that the above-described Fourier transform surrogate-based procedure does not perfectly reproduce the experimentally observed laser chaos time series, since the correlation in the above process is determined only by $r(t) = \lambda r(t - 1)$ in step (1), whereas experimental laser chaos involves very long-range time correlations via way of delayed optical feedback. However, we consider that the Fourier transform surrogate-based method is quite beneficial for the present study for several reasons.

First is that the correlations between two successive points can be specified by an arbitrary number, allowing λ values smaller than even -0.5 , which were experimentally not feasible, at least in the former studies [\[7,10\]](#). Therefore, systematic analysis is allowed concerning a wide range of λ . The second is that amplitude distributions are kept equivalent between each other

even when λ is configured in different values, which also allows us clear examination about the impact of autocorrelation inherent in the time series.

For these reasons, we use the time series $r'(t)$ generated by the above processes. We then analyze how the MAB performance depends on the autocorrelation specified by λ . In evaluating the performance of the MAB problem, we employ the *correct decision rate*, referred to as CDR hereafter. The $CDR(t)$ is defined as the ratio of selecting the slot machine with the highest reward probability at time step t , and averaged over m simulations or cycles. That is, $CDR(t)$ is expressed by

$$CDR(t) = \frac{1}{m} \sum_{i=1}^m C_i(t), \quad (3)$$

where m is the number of cycles with different random initial conditions. Here, $C_i(t) = 1$ when the slot machine with the highest reward probability is selected at the t -th decision (or time t) of the i -th cycle. Namely, correct decision-making was conducted. Otherwise, $C_i(t) = 0$, meaning that correct decision-making was not executed. In the following simulations, $m = 60000$.

Figure 2 summarizes the calculated CDR at $t = 1000$ as a function of the autocorrelation coefficient λ in several different reward environments and the setting of the decision-maker. The reward probability of the two slot machines, called machine A and machine B, is denoted by P_A and P_B . For example, in Figure 2(a), P_A and P_B are given by 0.9 and 0.3, respectively. In this situation, the correct decision is to select machine A since it is the highest reward probability slot machine ($P_A > P_B$). In addition, the number of the levels of threshold adjustor is five, specified by $N = 2$. It should be emphasized that the higher CDR is obtained when the autocorrelation is negative; indeed, the best CDR is given by $\lambda = -0.6$.

Figures 2(b) to 2(f) examine other reward settings and decision-maker conditions. Table 1 summarizes the reward probabilities of slot machines and the number of threshold levels N for each MAB problem. In Figures 2(b) and 2(c), while maintaining the threshold number the same as Figure 2(a) (that is, $N = 2$), P_A and P_B are differently configured. More specifically, the difference of P_A and P_B is only 0.1 in Figure 2(b) by setting $(P_A, P_B) = (0.6, 0.5)$. Similarly, the difference is 0.2 in Figure 2(c) by $(P_A, P_B) = (0.9, 0.7)$. That is, the difficulties in finding the best machine are configured differently. Here, what should be remarked is that the highest CDR is accomplished when the autocorrelation coefficient λ is given by -0.8 and -0.3 in Figures 2(b) and 2(c), respectively. That is, the best decision-making is realized with negatively correlated time series.

The reward setting of (P_A, P_B) of Figures 2(d), 2(e), and 2(f) is the same as Figures 2(a), 2(b), and 2(c), respectively. What is different is the threshold, which is specified by $N = 4$. The achieved CDR was different due to the change of N . However, it should be noted that the highest CDR performances are all obtained with negative autocorrelation when λ is given by -0.6 , -0.9 , and -0.6 in Figures 2(d), 2(e), and 2(f), respectively.

4. Theoretical Model of Decision Making Using Correlated Time Series

This section shows a mathematical model to account for the impact of correlated time series for decision-making. Here we focus on two-armed bandit problems where two slot machines are called machines A and B. Figure 3 shows a conceptual architecture of the proposed model.

We assume slot machine A has a larger reward probability than slot machine B; that is, $P_A > P_B$ holds. Therefore, the correct decision is to choose slot machine A.

Here, we assume that the subjected time sequence takes either of two signal levels specified by $+x$ or $-x$, which is denoted by sky blue marks in Figure 3. In the meantime, remember that the threshold level, $T(t)$ given by equation (1), takes in total $2N + 1$ different signal levels, each of which is represented by $-N, -N + 1, \dots, N - 1, N$. Furthermore, we suppose that the higher-level signal $+x$ satisfies $N - 1 < x < N$, meaning that the upper signal level of the incoming time series is below the maximum threshold level but greater than the second maximum threshold. Similarly, the lower signal level ($-x$) satisfies $-N < -x < -N + 1$, indicating that the lower signal level of the subjected time series is above the minimum threshold level but less than the second minimum threshold.

Based on the decision-making principle described in Section 2, we summarize how the decision-making is conducted in the present situation. Let the signal level of the incoming time series at time t and the threshold level at time t be denoted by $T(t)$ and $s(t)$, respectively.

- If $T(t) = -N$, regardless of the signal level $s(t)$, slot machine A is selected. This is because $T(t) = -N < s(t)$ always holds since the minimum of $s(t)$ is $-x$, which is larger than $-N$.
- Similarly, if $T(t) = N$, slot machine B is selected regardless of the signal level of $s(t)$ because $T(t) = N > s(t)$ always holds since the maximum of $s(t)$ is $+x$, which is smaller than N .
- If $-N + 1 \leq T(t) \leq N - 1$, the decision of selecting slot machine A or B depends on the signal level of $s(t)$.
 - If $s(t)$ is given by $+x$, the decision is to select machine A because $s(t) = +x$ is greater than $N - 1$.
 - Conversely, if $s(t)$ is given by $-x$, the decision is to select machine B because $s(t) = -x$ is smaller than $-N + 1$.

Furthermore, the incoming signal $s(t)$ contains inherent correlations, as discussed in Sections 1 and 2. Concerning the fact that $s(t)$ under study is a two-level signal train, we can think of the probability where the signal level $s(t + 1)$ at time $t + 1$ is different from $s(t)$ at time t ; that is, $s(t + 1) = +x$ results after $s(t) = -x$ or $s(t + 1) = -x$ after $s(t) = +x$. Since the autocorrelation between two consecutive timing is given by λ , such a signal level changing probability is given by $\mu = (1 - \lambda)/2$. Conversely, the probability of exhibiting the same signal level is given by $1 - \mu = (1 + \lambda)/2$.

Therefore, such stochastic processes are represented by conditional probabilities given by

$\Pr(s(t + 1) = \pm x \mid s(t) = \mp x) = \mu$ and $\Pr(s(t + 1) = \pm x \mid s(t) = \pm x) = 1 - \mu$, (4) where \Pr denotes probability. What is important is that the internal status of the decision-maker, represented by $T(t)$, is tightly coupled with the correlated time series subjected to the system as well as the betting results of the slot machine playing, which is specified by P_A and P_B .

The behavior of the revision of $T(t)$ is described by the following cases:

- If $T(t) = -N$, slot machine A is always selected. The threshold is updated by
$$T(t + 1) = \begin{cases} T(t) + 1 & (\text{when machine A fails with probability } 1 - P_A) \\ T(t) & (\text{when machine A wins with probability } P_A) \end{cases}.$$
- If $T(t) = N$, slot machine B is always selected. The threshold is updated by

$$T(t+1) = \begin{cases} T(t) & \text{(when machine B wins with probability } P_B) \\ T(t) - 1 & \text{(when machine B fails with probability } 1 - P_B) \end{cases}$$

- If $-N \leq T(t) \leq N - 1$,

In the case when slot machine A is selected, the threshold is updated by

$$T(t+1) = \begin{cases} T(t) + 1 & \text{(when machine A fails with probability } 1 - P_A) \\ T(t) - 1 & \text{(when machine A wins with probability } P_A) \end{cases},$$

In the case when slot machine B is selected, the threshold is updated by

$$T(t+1) = \begin{cases} T(t) + 1 & \text{(when machine B wins with prob. } P_B) \\ T(t) - 1 & \text{(when machine B fails with prob. } 1 - P_B) \end{cases}.$$

It should be remarked that regardless of the machine selection and betting result, the threshold level always increases or decreases in this case, meaning that the identical threshold level is not allowed.

The procedure summarized above a special case of the principle shown in [Section 2](#) by specifying the parameters therein by $k = \Delta = \Omega = \alpha = 1$. In addition, we have to emphasize that the upper and the lower limit of $T(t)$ is newly posed: when the decrement or increment of the threshold is not permitted beyond the range between $-N$ and N . In the following, we call this the stopping rule.

To theoretically deal with the abovementioned seemingly complex situations, we introduce a set $\mathbf{v}_t = (T(t), s(t))$, which represents the state of the model at time t . The space spanned by \mathbf{v}_t is $\{-N, -N + 1, \dots, N - 1, N\} \times \{\pm x\}$.

Herein, we can characterize state transition probability between two states. Let, for example, the current state is specified by $(i, +x)$ while $T(t)$ is not at the border; i.e., $-N + 1 \leq i \leq N - 1$. Here we consider the probability of the state transition to $(i + 1, -x)$. It should be noted that the decision is to select machine A in this situation $(i, +x)$ since the signal level $+x$ is larger than the current threshold $T(t)$. In this state transition from $(i, +x)$ to $(i + 1, -x)$, the threshold is incremented ($i \rightarrow i + 1$) and the incoming signal level is reversed ($+x \rightarrow -x$). Such a situation occurs when the slot machine A playing is failed as well as the incoming signal level is flipped, of which probability is given by $(1 - P_A)\mu$. Similarly, all transition probabilities are determined.

The notion of correlated random walk allows us to summarize such transitions in a unified manner [\[22,23\]](#). We first introduce the probability of the state \mathbf{v}_t by $\pi_t(\mathbf{v}) = \pi_t(i, \sigma)$, meaning the probability of the state with $T(t) = i$ and $s(t) = \sigma$. In addition, we define a probability vector $\boldsymbol{\pi}_t(i)$ given by

$$\boldsymbol{\pi}_t(i) = \begin{bmatrix} \pi_t(i, +x) \\ \pi_t(i, -x) \end{bmatrix}, \quad (5)$$

which combines probabilities involving the threshold level being i but the signal level of the time series is different ($+x$ and $-x$).

We denote the probability of the threshold being i at time t , regardless of the incoming signal level, by $\pi_t(i)$, which is mathematically equivalent to the L^1 -norm of $\boldsymbol{\pi}_t(i)$. That is,

$$\pi_t(i) = \pi_t(i, +x) + \pi_t(i, -x) = |\pi_t(i, +x)|_1 + |\pi_t(i, -x)|_1 = \|\boldsymbol{\pi}_t(i)\|_1. \quad (6)$$

Based on these preparations, recurrent formulae of $\boldsymbol{\pi}_t(i)$ leads us to precisely characterize the behavior of the system.

[CASE 1]

The probability vector regarding the cases when the threshold is between $-N + 1$ and $N - 1$ at time $t + 1$ is given by

$$\boldsymbol{\pi}_{t+1}(i) = \mathbf{Q}(i-1)\boldsymbol{\pi}_t(i-1) + \mathbf{P}(i+1)\boldsymbol{\pi}_t(i+1), \quad (7)$$

where the matrices \mathbf{P} and \mathbf{Q} are given by

$$\mathbf{P}(i) = \begin{bmatrix} P_A(1-\mu) & (1-P_B)\mu \\ P_A\mu & (1-P_B)(1-\mu) \end{bmatrix} \quad (8)$$

$$\mathbf{Q}(i) = \begin{bmatrix} (1-P_A)(1-\mu) & P_B\mu \\ (1-P_A)\mu & P_B(1-\mu) \end{bmatrix}. \quad (9)$$

Equation (7) clearly implies that the probability vector of the threshold being i consists of the transitions from the states with the threshold being $i - 1$ and $i + 1$. The elements of the matrices $\mathbf{P}(i)$ and $\mathbf{Q}(i)$ are intuitively easily understood by the following. The dynamics given by equation (7) are schematically illustrated in Figure 4(a).

The matrix $\mathbf{P}(i)$ concerns the probability of *decrementing* the threshold level. For example, the (1,1)-element of $\mathbf{P}(i)$, or $\mathbf{P}_{1,1}(i)$, represents the probability of the transition from the state $(i, +x)$ to $(i - 1, +x)$. The state $(i, +x)$ indicates that the decision is to select machine A. The decrement of the threshold means that the result is a win. The probability of consecutive identical signal levels is given by $1 - \mu$. Hence, $\mathbf{P}_{1,1}(i) = P_A (1 - \mu)$. Similarly, $\mathbf{P}_{1,2}(i)$ means the probability of the transition from the state $(i, -x)$ to $(i - 1, +x)$; the difference is the change of the polarity of the incoming signal level. Therefore, $\mathbf{P}_{1,2}(i) = (1 - P_B) \mu$. The $\mathbf{P}_{2,1}(i)$ corresponds to the probability of the transition from the state $(i, +x)$ to $(i - 1, -x)$, and $\mathbf{P}_{2,2}(i)$ means that from $(i, -x)$ to $(i - 1, -x)$. The blue arrows in Figure 4(a) schematically represent the role of the matrix $\mathbf{P}(i)$, which concerns the decrementing of the threshold level.

Conversely, the matrix $\mathbf{Q}(i)$ concerns the probability of *incrementing* the threshold level. $\mathbf{Q}_{1,1}(i)$, for example, represents the probability of the transition from the state $(i, +x)$ to $(i + 1, +x)$, meaning that the threshold is incremented while the signal level is unchanged. This situation represents the decision is to select machine A, the result is lost, and the polarity of the incoming signal is the same; the corresponding probability is given by $(1 - P_A)(1 - \mu)$. Similarly, other elements of $\mathbf{Q}(i)$ are specified in a straightforward manner. The red arrows in Figure 4(a) schematically represent the role of the matrix $\mathbf{Q}(i)$, which concerns the incrementing of the threshold level.

[CASE 2]

The probability vector regarding the case when the threshold is at the edge on the negative side, $-N$ at time $t + 1$ is specified by

$$\boldsymbol{\pi}_{t+1}(-N) = \mathbf{P}(-N)\boldsymbol{\pi}_t(-N) + \mathbf{P}(-N + 1)\boldsymbol{\pi}_t(-N + 1). \quad (10)$$

We need some careful treatment at the edges. First, $\mathbf{P}(-N + 1)$ in the second term on the right-hand side of equation (10) describes the transition of the decrement of the threshold level from $-N + 1$ to N , which has been already defined by equation (8). Second, since there are no threshold levels smaller than $-N$, the transitions involving increments or any \mathbf{Q} matrix is not included in equation (10). Third, what is different from CASE 1 above is that the threshold level can be maintained at the edge, which is indicated by the first term on the right-hand side of equation (10). More specifically, the \mathbf{P} matrix at $-N$ is given by

$$\mathbf{P}(-N) = \begin{bmatrix} P_A(1-\mu) & P_A\mu \\ P_A\mu & P_A(1-\mu) \end{bmatrix}. \quad (11)$$

$\mathbf{P}_{1,1}(-N)$ means the state transition from $(-N, +x)$ to $(-N, +x)$. This corresponds to the selection is machine A, and the result is winning, and the signal polarity is unchanged. Therefore $\mathbf{P}_{1,1}(-N) = P_A (1 - \mu)$. Similarly, $\mathbf{P}_{1,2}(-N)$ means the state transition from $(-N, -x)$ to $(-N, +x)$;

what is different from $P_{1,1}(-N)$ is the change of the polarity. Hence, $P_{1,2}(-N) = P_A \mu$. Likewise, $P_{2,1}(-N)$ and $P_{2,2}(-N)$ are obtained. The blue arrows in Figure 4(b) illustrates the role of the matrix $P(-N)$, which concerns keeping the identical threshold level.

[CASE 3]

Similarly to CASE 2, the probability vector regarding the case when the threshold is N at time $t + 1$ is specified by

$$\pi_{t+1}(N) = Q(N-1)\pi_t(N-1) + Q(N)\pi_t(N). \quad (12)$$

The meaning of equation (12) is similar to equation (10). $Q(N-1)$ in the right-hand side of equation (12) has been already defined by equation (9). As in CASE 2, the threshold level can be maintained at the edge, which is shown by $Q(N)$ in equation (12). This is given by

$$Q(N) = \begin{bmatrix} P_B(1-\mu) & P_B\mu \\ P_B\mu & P_B(1-\mu) \end{bmatrix}. \quad (13)$$

$Q_{1,1}(N)$ means the state transition from $(N, +x)$ to $(N, +x)$. This corresponds to the selection is machine B, and the result is winning, and the signal polarity is unchanged. Therefore $Q_{1,1}(N) = P_B(1-\mu)$. Similarly, $Q_{1,2}(N)$ means the state transition from $(N, -x)$ to $(N, +x)$; what is different from $Q_{1,1}(N)$ is the change of the polarity. Hence, $Q_{1,2}(N) = P_B\mu$. Likewise, $Q_{2,1}(N)$ and $Q_{2,2}(N)$ are obtained. The red arrows in Figure 4(c) illustrate the role of the matrix $Q(N)$, which concerns keeping the same threshold level.

Finally, a remark is needed for the P matrix at N and the Q matrix at $-N$, which should be different from the one given by equations (8) and (9), and are given by

$$P(N) = \begin{bmatrix} (1-P_B)(1-\mu) & (1-P_B)\mu \\ (1-P_B)\mu & (1-P_B)(1-\mu) \end{bmatrix}, \quad (14)$$

$$Q(-N) = \begin{bmatrix} (1-P_A)(1-\mu) & (1-P_A)\mu \\ (1-P_A)\mu & (1-P_A)(1-\mu) \end{bmatrix}. \quad (15)$$

This is because the decision at the edges does not depend on the incoming signal level. For example, with the threshold at N , the decision is always to select machine B because both signal level $+x$ and $-x$ is smaller than the threshold. Hence $P_{1,1}(N)$ means the probability of the state transition from $(N, +x)$ to $(N-1, +x)$, meaning that the decision is to select machine B, the result is lost, and the polarity of the signal is unchanged. Therefore $P_{1,1}(N) = (1-P_B)(1-\mu)$. Similarly, all other elements in equations (14) and (15) are specified. The blue arrows in Figure 4(c) and the red arrows in Figure 4(b) illustrates $P(N)$ and $Q(-N)$, respectively.

Figure 5 summarizes the chains of the probability vector $\pi_t(i)$ by equations (7), (10), and (12). The blue arrows, which regard the decrement of the threshold level, are induced by either the winning by selecting machine A or lost by selecting machine B. In contrast, the red arrows, which represent the increment of the threshold level, are triggered by either the winning by selecting machine B or lost by selecting machine A. At the same time, the thresholds at the edge ($-N$ and N) involve identity allows.

Finally, the CDR can be discussed by way of the probabilities defined above. Assume that the correct decision is to select machine A. The selection of machine A is realized excessively by the following two cases:

1. The threshold is $-N$. In this case, both signal levels $-x$ and $+x$ lead to the decision of choosing machine A.
2. When the threshold is between $-N+1$ and $N-1$, the input signal level of $+x$ provides the decision of selecting machine A.

Hence, the probability of selecting machine A at time t , denoted by $CDR^{(\text{theory})}(t)$, is given by

$$CDR^{(theory)}(t) = \pi_t(-N, -x) + \pi_t(-N, +x) + \sum_{i=-N+1}^{N-1} \pi_t(i, +x). \quad (16)$$

5. Evaluation

With the theoretical model shown in [Section 4](#), we can calculate the time evolution of the probability vector $\pi_t(i)$ and its L^1 -norm $\pi_t(i)$ from any initial conditions; and consequently, $CDR^{(theory)}(t)$ is derived by [equation \(16\)](#).

Here we examine the case where the reward probabilities are given by $P_A = 0.9$ and $P_B = 0.7$ and assume that N is given by 2, meaning that the number of threshold levels is 5. Herein, the initial probability vector is given by $\pi_1(0) = (0.5, 0.5)$ while assuming all the other vectors are zero. The autocorrelation coefficient λ specifies the time-correlated, two-level signal trains.

[Figure 5\(b\)](#) shows the analytically calculated chains of probability vectors. As time evolves, the probability vector at the edge ($i = -2$) increases, indicating the high likelihood of choosing machine A, which is the correct decision (since $P_A > P_B$).

To examine the mechanism more deeply, [Figures 6\(a\), 6\(b\), and 6\(c\)](#) demonstrate the time evolution of the probability when the threshold is at level i ($i = -2, -1, 0, 1, 2$) when the autocorrelation λ is specified by $-0.8, 0$, and 0.8 , respectively. What is commonly observed is in these figures is that $\pi_t(-2)$, which is indicated by blue curves, increases as the time elapses, leading to the high chances of selecting machine A or correct decision-making. Meanwhile, $\pi_t(2)$ values, indicated by green curves, exhibits approximately 0.2 at the time step of 25 when λ is given by 0.8 ([Figure 6\(c\)](#)), whereas it shows nearly zero at the same timing when λ is given by -0.8 ([Figure 6\(a\)](#)). That is to say, the probability of choosing machine B, which is the wrong decision, is not negligible when $\lambda = 0.8$.

From another perspective, the blue, red, and yellow markers in [Figure 6\(d\)](#) characterize the probabilities of the threshold at $t = 1000$, which is written by $\pi_{1000}(i)$, when the autocorrelation is specified by λ is given by $-0.8, 0$, and 0.8 respectively. We can clearly observe a large probability greater than 0.6 about the threshold level of -2 , regardless of λ values.

It is remarkable that, with $\lambda = -0.8$, the probability monotonically decreases as the threshold increases, whereas with $\lambda = 0.8$, the probability increases when the threshold increases from 0 to 2. Even with zero autocorrelation ($\lambda = 0$), a slight increase in probability is observed at the threshold level of 2. We consider that the positive autocorrelation tends to conduct similar decisions consecutively, and hence the decision can be locked in a status, which is actually not the optimal one. Indeed, a related tendency is observed in [Figures 6\(a\), 6\(b\), and 6\(c\)](#), where the dynamic change of probabilities, most notably by $\pi_t(0)$ indicated by orange curves, exhibit a strong oscillatory behavior with $\lambda = -0.8$, whereas it is attenuated when $\lambda = 0.8$.

As discussed in [Section 4](#), the decision-making ability can be theoretically derived as $CDR^{(theory)}(t)$ given by [equation \(16\)](#) through the probability model. We examined $CDR^{(theory)}(t)$ depending on a variety of conditions. Herein, the reward probabilities (P_A, P_B)

and the number of threshold levels specified by N are summarized in Table 1, which are the same as the discussions in Section 3 and Figure 2. For example, Figure 7(a) concerns the case $(P_A, P_B) = (0.9, 0.3)$ and $N = 2$. The red curves in Figure 7 show $CDR^{(theory)}(1000)$ as a function of autocorrelation coefficient λ ranging from -0.95 to 0.9 with 0.05 interval. In addition, $\lambda = -0.99$ is examined. For all cases in Figure 7, the maximum $CDR^{(theory)}(1000)$ are obtained when the autocorrelation coefficient is negative, indicated by red arrows therein, which coincides with the numerical observations shown in Figure 2.

Furthermore, we numerically simulate correct decision rate $CDR(t)$ defined by equation (3) based on the original decision-making algorithm described in Section 3 while adapting the stopping rule in Section 4; the results are shown by the blue curves in Figure 7. We observe in all panels in Figure 7 that the theory (red) and the simulation (blue) are matched well with each other. Also, while the blue marks exhibit fluctuations since they are obtained as a statistical average via numerical results, the results by red marks are smooth because they are analytically derived based on the theory in Section 4.

6. Conclusion

In this study, we construct the theoretical model to account for the acceleration of decision-making by correlated time sequences. The former studies have shown that the solution of the two-armed bandit problem is accelerated by negative autocorrelation inherent in the time series subjected to the decision-making system. However, its underlying mechanisms are not understood. We begin the discussion by clarifying the impact of time-domain correlation on decision-making by utilizing time series with specific autocorrelation designed via Fourier transform surrogate. Coinciding with the prior reports using experimentally observed laser chaos time series, we confirm that the negative autocorrelation accomplishes superior decision-making performance. The difficulties of understanding the underlying mechanism of such acceleration stem from the fact that multiple entities are involved; the dynamical reconfiguration of the internal status of the decision-maker (the threshold level and its revision), the time-domain structure of the incoming time series, and the stochastic attributes of the environment (reward probability of slot machines). The theoretical model of this study unifies these entities based on correlated random walks. Furthermore, the decision-making performance obtained analytically by the theoretical model agrees with the numerical results by simulations, which validates the proposed theory. Also, this indicates that the optimal autocorrelation for maximizing can be obtained through the model without executing enormous numerical simulations. This paper constitutes a foundation of the intellectual mechanism enhanced by correlated time series, which is important for future information and communications technology.

Conflicts of Interest

The authors declare that they have no conflicts of interest.

Acknowledgments

This work was supported in part by the CREST project (JPMJCR17N2) funded by the Japan Science and Technology Agency and Grants-in-Aid for Scientific Research (JP20H00233) funded by the Japan Society for the Promotion of Science.

References

- [1] B. J. Shastri, A. N. Tait, T. Ferreira de Lima, W. H. Pernice, H. Bhaskaran, C. D. Wright, and P. R. Prucnal, “Photonics for artificial intelligence and neuromorphic computing,” *Nature Photonics*, vol. 15, pp. 102–114, 2021.
- [2] G. Wetzstein, A. Ozcan, S. Gigan, S. Fan, D. Englund, M. Soljačić, C. Denz, D. A. B. Miller, and D. Psaltis, “Inference in artificial intelligence with deep optics and photonics,” *Nature*, vol. 588, no. 7836, pp. 39–47, 2020.
- [3] Z. Chen and M. Segev, “Highlighting photonics: looking into the next decade,” *eLight*, vol. 1, art. no. 2, 2021.
- [4] G. Genty, L. Salmela, J. M. Dudley, D. Brunner, A. Kokhanovskiy, S. Kobtsev, and S. K. Turitsyn, “Machine learning and applications in ultrafast photonics,” *Nature Photonics*, vol. 15, no. 2, pp. 91–101, 2021.
- [5] K. Kitayama, M. Notomi, M. Naruse, K. Inoue, S. Kawakami, and A. Uchida, “Novel frontier of photonics for data processing—Photonic accelerator,” *APL Photonics*, vol. 4, no. 9, art. no. 090901, 2019.
- [6] R. S. Sutton and A. G. Barto, *Introduction to reinforcement learning*, MIT press, Cambridge, USA, 1998.
- [7] M. Naruse, Y. Terashima, A. Uchida, and S.-J. Kim, “Ultrafast photonic reinforcement learning based on laser chaos,” *Scientific Reports*, vol. 7, art. no. 8772, 2017.
- [8] M. Naruse, N. Chauvet, A. Uchida, A. Drezet, G. Bachelier, S. Huant, and H. Hori, “Decision making photonics: solving bandit problems using photons,” *IEEE Journal of Selected Topics in Quantum Electronics*, vol. 26, no. 1, art. no. 7700210, 2020.
- [9] J. Bueno, S. Maktoobi, L. Froehly, I. Fischer, M. Jacquot, L. Larger, and D. Brunner, “Reinforcement learning in a large-scale photonic recurrent neural network,” *Optica*, vol. 5, no. 6, pp. 756–760, 2018.
- [10] M. Naruse, T. Mihana, H. Hori et al., “Scalable photonic reinforcement learning by time-division multiplexing of laser chaos,” *Scientific Reports*, vol. 8, art. no. 10890, 2018.
- [11] S. Takeuchi, M. Hasegawa, K. Kanno et al., “Dynamic channel selection in wireless communications via a multi-armed bandit algorithm using laser chaos time series,” *Scientific Reports*, vol. 10, art. no. 1574, 2020.
- [12] H. Kanemasa, A. Li, Y. Ito et al., “Dynamic channel bonding in WLANs by hierarchical laser chaos decision maker,” *Nonlinear Theory and Its Applications*, vol. 13, no. 1, pp. 84–100, 2022.
- [13] Z. Duan, A. Li, N. Okada et al., “User pairing using laser chaos decision maker for NOMA systems,” *Nonlinear Theory and Its Applications* vol. 13, no. 1, pp. 72–83, 2022.
- [14] K. Kanno, M. Naruse, and A. Uchida, “Adaptive model selection in photonic reservoir computing by reinforcement learning,” *Scientific Reports*, vol. 10, no. 10062, 2020.
- [15] L. Lai, H.E. Jiang, and H.V. Poor, “Cognitive medium access: Exploration, exploitation, and competition,” *IEEE Transactions on Mobile Computing*, vol. 10, no. 2, pp. 239–253, 2011.
- [16] N. Okada, M. Hasegawa, N. Chauvet, A. Li, and M. Naruse, “Analysis on Effectiveness of Surrogate Data-Based Laser Chaos Decision Maker,” *Complexity*, vol. 2021, art. no. 8877660, 2021.
- [17] G. Mazzini, R. Rovatti, and G. Setti, “Interference minimisation by auto-correlation shaping in asynchronous DS-CDMA systems: chaos-based spreading is nearly optimal,” *Electronics Letters*, vol. 35, no 13, pp. 2256–2262, 1999.
- [18] T. Kohda, and H. Fujisaki, “Pursley’s aperiodic cross-correlation functions revisited,” *IEEE Transactions on Circuits and Systems I: Fundamental Theory and Applications*, vol. 50, no. 6, pp. 800–805, 2003.

- [19] M. Hasegawa, “Improving Performance of Heuristic Algorithms by Lebesgue Spectrum Filter,” *IEICE Trans. Communications*, vol. E99–B, no. 11, pp. 2256–2262, 2016.
- [20] K. Umeno, and A. Yamaguchi, “Construction of optimal chaotic spreading sequence Using Lebesgue Spectrum Filter,” *IEICE Trans. Fundamentals*, vol. E85–A, no. 4, pp.849–852, 2002.
- [21] H. Watanabe, Y. Narumiya, and M. Hasegawa, “Performance evaluation of chaotic CDMA using an implemented system on software defined radio,” *Nonlinear Theory and Its Applications*, vol. 4, no. 4, pp. 473–481, 2013.
- [22] E. Renshaw and R. Henderson, “The correlated random walk,” *Journal of Applied Probability*, vol. 18, no. 2, pp. 403–414, 1981.
- [23] N. Konno, “Limit theorems and absorption problems for one-dimensional correlated random walks,” *Stochastic Models*, vol. 25, no. 1, pp. 28–49, 2009.
- [24] J. Theiler, S. Eubank, A. Longtin, B. Galdrikian, and J. D. Farmer, “Testing for nonlinearity in time series: the method of surrogate data,” *Physica D*, vol. 58, pp. 77–94, 1992.

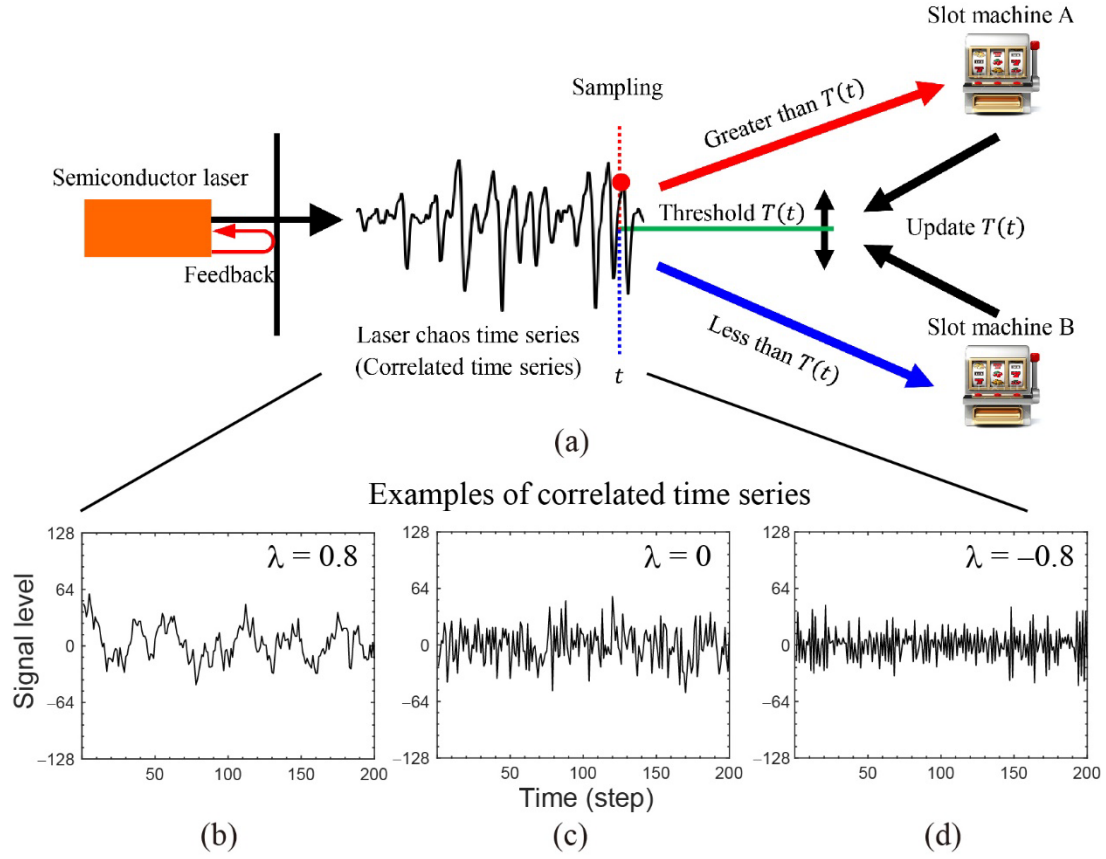


Figure 1: (a) The decision-making architecture using laser chaos time series or correlated time series. (b, c, d) Snapshots of correlated time series generated via Fourier transform surrogate. The correlation is specified by the parameter λ . (a) $\lambda = 0.8$ (strong positive autocorrelation), (b) $\lambda = 0$ (zero correlation) (c) $\lambda = -0.8$ (strong negative autocorrelation).

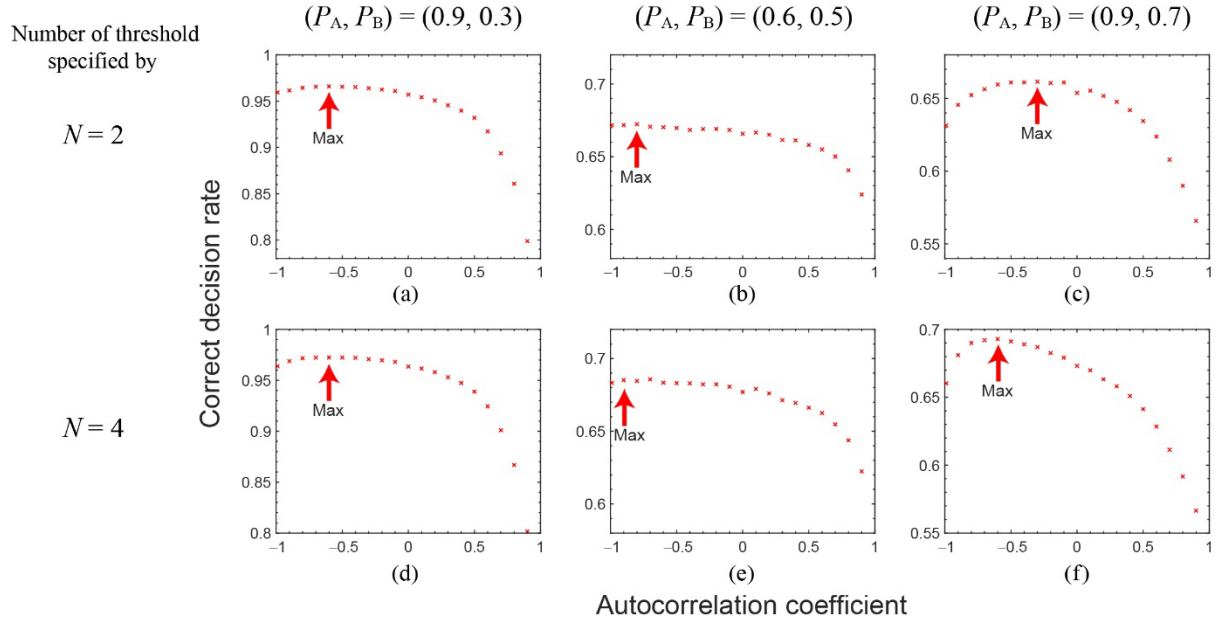


Figure 2: Correct decision rate at $t = 1000$ as a function of the autocorrelation coefficient λ in various reward environments and a different number of threshold levels. What is remarkable is that the maximum performance is obtained all by negatively correlated time series. (a) $P_A = 0.9, P_B = 0.3, N = 2$ (b) $P_A = 0.6, P_B = 0.5, N = 2$ (c) $P_A = 0.9, P_B = 0.7, N = 2$ (d) $P_A = 0.9, P_B = 0.3, N = 4$ (e) $P_A = 0.6, P_B = 0.5, N = 4$ and (f) $P_A = 0.9, P_B = 0.7, N = 4$.

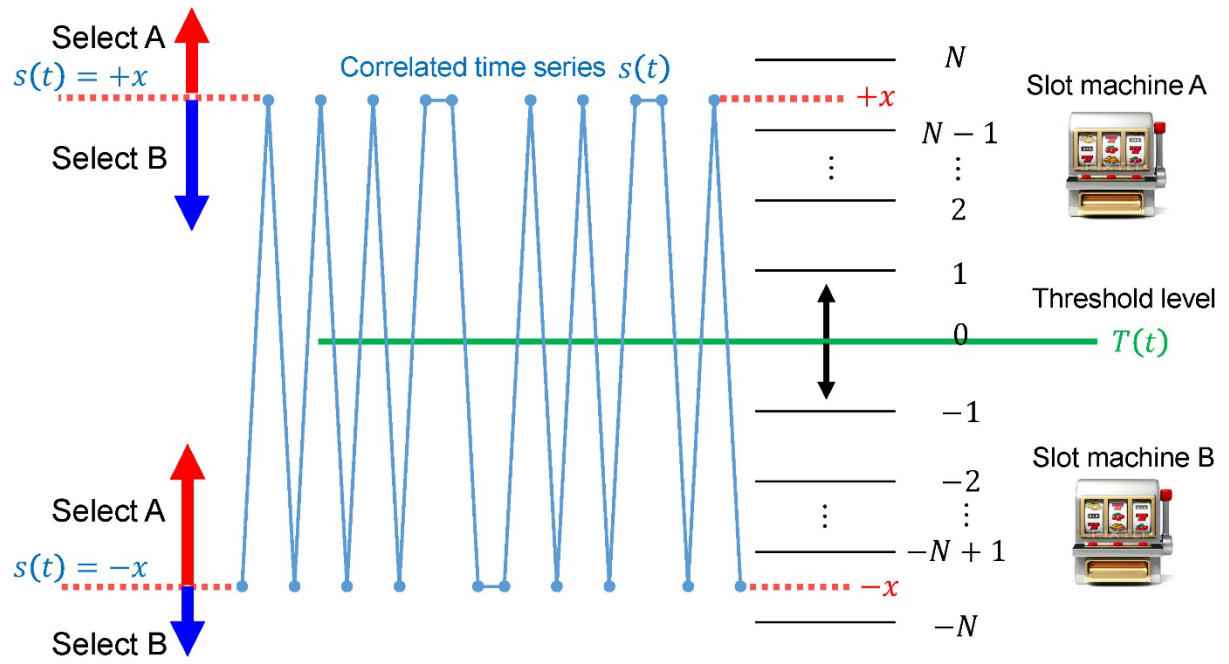


Figure 3: The theoretical model of the decision-making based on correlated time series and reconfiguration of the threshold.

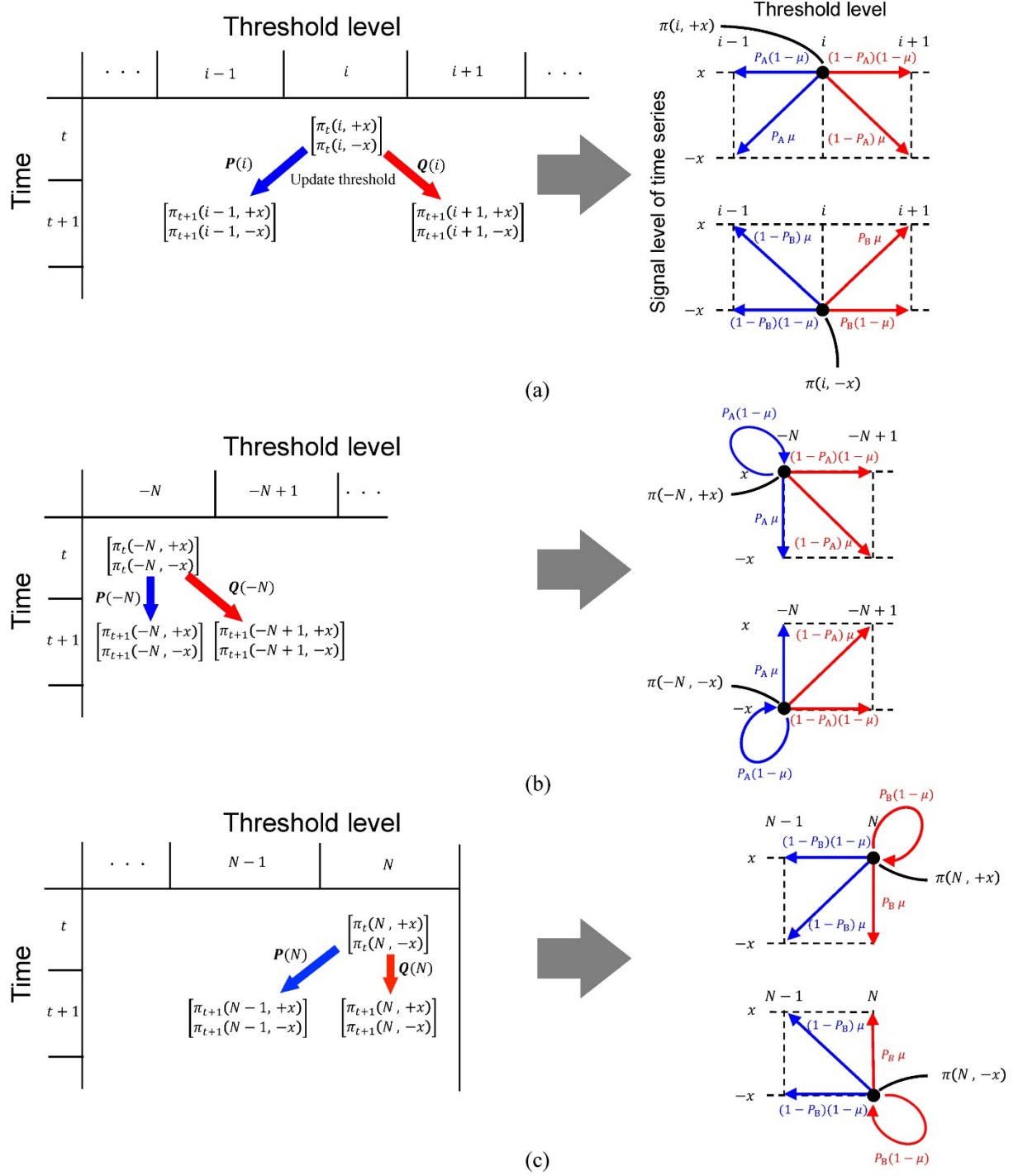


Figure 4: Transitions probability vectors of the model. (a) The matrices of P and Q concern the increment and decrement of the threshold level. (b, c) When the threshold is at the edge ($-N$ or N), transitions to an identical threshold should be considered, which are represented by $P(-N)$ and $Q(N)$ in (b) and (c), respectively.

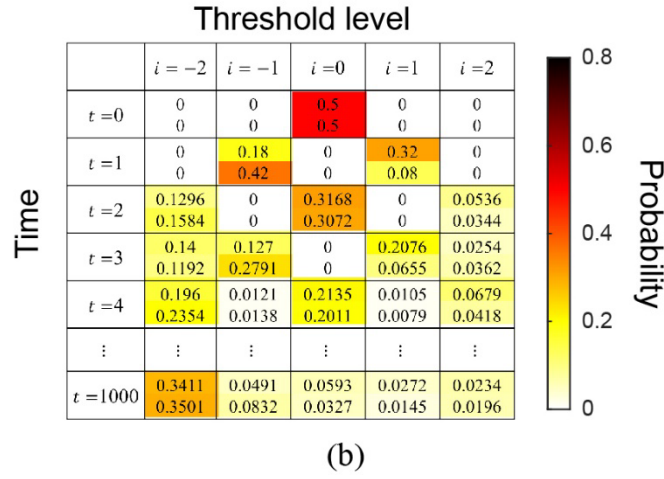
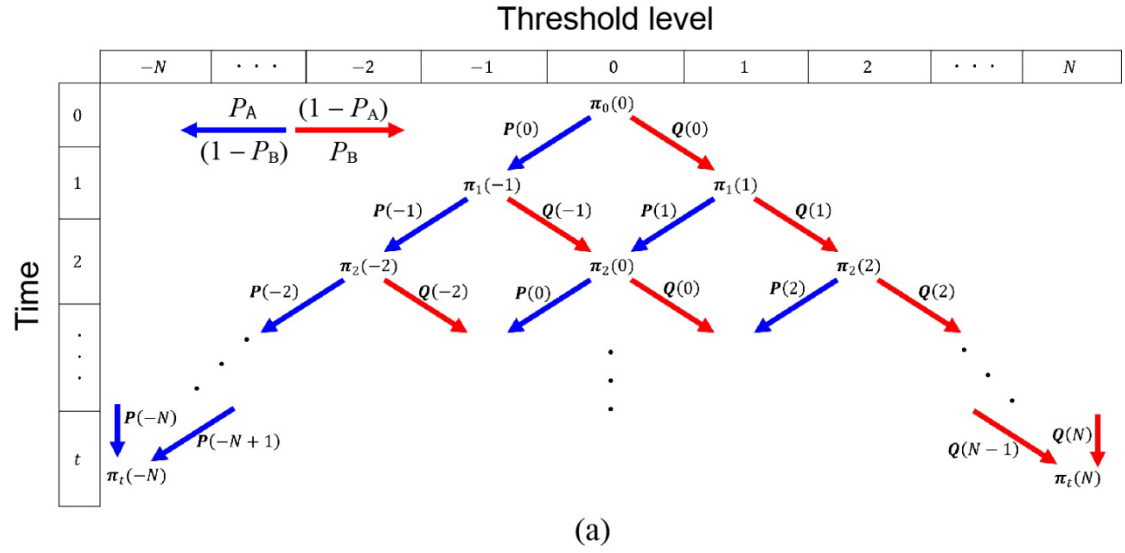


Figure 5: (a) Chains of the probability vector $\pi_t(i)$ given by equations (7), (10), and (12). (b) An example of the evolution of probability vector $\pi_t(i)$ when the initial condition is $\pi_0(0) = (0.5, 0.5)$, the autocorrelation coefficient λ is -0.8 , the threshold number is specified by $N = 2$, and the reward environment is $(P_A, P_B) = (0.9, 0.7)$.

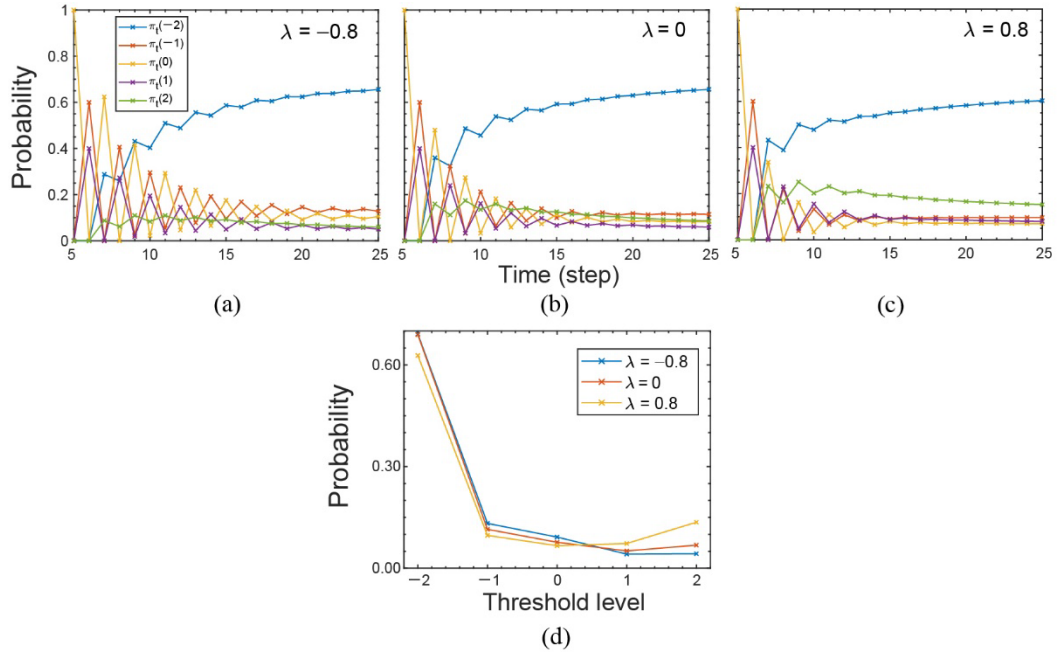


Figure 6: (a,b,c) The time evolution of the probabilities that occupy each of the threshold levels. The reward probabilities are given by $(P_A, P_B) = (0.9, 0.7)$. The autocorrelation coefficient λ is configured differently: (a) $\lambda = -0.8$, (b) $\lambda = 0$, and (c) $\lambda = 0.8$. (d) Comparison of the probabilities occupying threshold level with different autocorrelation coefficients at $t = 1000$.

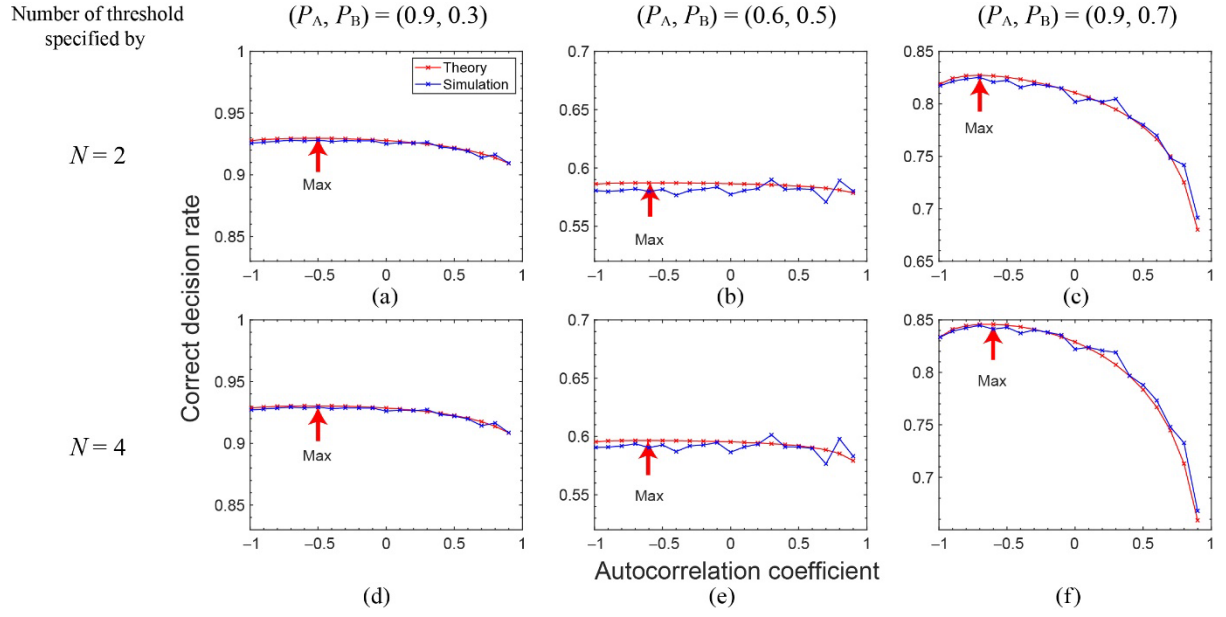


Figure 7: Correct decision rate at $t = 1000$ derived by the proposed theoretical model (red) and numerical simulations (blue) as a function of the autocorrelation coefficient λ . The reward probability settings and the number of threshold levels are the same with Figure 2. The threshold level is specified by $N=2$ in (a), (b), and (c) whereas $N=4$ in (d), (e), and (f). In (a) and (d), the reward probability is given by $(P_A, P_B) = (0.9, 0.3)$. In (b) and (e), $(P_A, P_B) = (0.6, 0.5)$. In (c) and (f), $(P_A, P_B) = (0.9, 0.7)$.

Table 1: The settings of the reward probabilities of slot machines (P_A and P_B) and the parameter N that specifies the number of threshold levels ($2N + 1$).

Figure	P_A	P_B	N
2(a), 7(a)	0.9	0.3	2
2(b), 7(b)	0.6	0.5	2
2(c), 7(c)	0.9	0.7	2
2(d), 7(d)	0.9	0.3	4
2(e), 7(e)	0.6	0.5	4
2(f), 7(f)	0.9	0.7	4